2019 IEEE International Ultrasonics Symposium (IUS)
Glasgow, Scotland, October 6-9, 2019

# The role of primary and secondary acoustic radiation forces on the contactless manipulation of liquid droplets in mid-air

Marco A. B. Andrade
*Institute of Physics*
*University of São Paulo*
São Paulo, Brazil
marcobrizzotti@gmail.com

Gergely Simon
*OnScale Ltd*
Glasgow, UK
gergely.simon@onscale.com

Anne Bernassau
*School of Engineering and Physical Sciences*
*Heriot-Watt University*
Edinburgh, UK
a.bernassau@hw.ac.uk

Asier Marzo
*Computer Science*
*Public University of Navarre*
Pamplona, Spain
asier.marzo@unavarra.es

***Abstract*—The primary and the secondary acoustic radiation forces acting on water droplets are investigated in a multifocal point acoustic levitator consisting of an array of 256 ultrasonic transducers on top of a plane reflector. Two water droplets are levitated separately and manipulated horizontally until they coalesce. The motion of each droplet is captured by a high-speed camera and a tracking algorithm is used for determining the position of each droplet over time. From positions of each droplet over time, a numerical procedure is used for determining the acoustic radiation force acting on each droplet. In addition, the primary force is simulated by a numerical model that combines a matrix method with the Gor'kov equation and the secondary force is calculated through simulations using the Finite Element Method.**

***Keywords—acoustic levitation, acoustic tweezer, acoustic radiation force, standing wave***

## I. INTRODUCTION

The contactless suspension of objects with sound waves is called acoustic levitation [1], [2]. The acoustic levitation method is based on the phenomenon of acoustic radiation pressure [3], [4], which arises from the transfer of momentum transported by the wave to the object. One of the greatest advantages of acoustic levitation in comparison with other levitation techniques (e.g. magnetic, electrostatic etc.) relies in the possibility of levitating a wide range of materials. This allows the levitation of solids [5], [6], liquids [7], soap bubbles [8] and even living insects [9].

The most common approach for acoustically suspending objects in mid-air uses standing wave fields, in which objects much smaller than the acoustic wavelength are trapped at the pressure nodes of the standing wave. In this type of acoustic levitation, a standing wave field is normally generated between an emitter and a reflector [10]–[12], two opposing emitters [13], or between arrays of transducers [14]–[17]. Acoustic levitation based on standing waves allows not only suspending but also offers manipulation capability in one [13], [15], [18], two [19], [20], and three dimensions [14], [17].

This study was supported by the São Paulo Research Foundation (FAPESP – grant no. 2017/27078-0).

Perhaps one of the most important uses for acoustic levitation is related to the contactless manipulation of liquid droplets, which has a great potential in areas such as chemistry [21], pharmacy [22] and biology [23]. For instance, acoustic levitation can be used in X-diffraction experiments for determining the structure of proteins [24], [25] or it can be combined with Raman spectroscopy to investigate the crystallization process in levitating droplets [26]. Recent advances in acoustic levitation allow to manipulate and merge multiple droplets individually [19], [23], [27], [28].

When a single droplet levitates in an acoustic field, it experiences the primary acoustic radiation force originating from the incident acoustic field on the droplet. For multiple droplets, they also experience the secondary acoustic radiation force (also called interparticle force or Bjerknes force) [29]–[31] caused by the wave scattering by the adjacent droplets. Secondary forces are of great importance when merging droplets, since they cause an attractive force between the droplets that contributes to the coalescence process.

In this study, the primary and secondary radiation forces acting on levitated droplets are investigated numerically and experimentally. Water droplets are levitated and merged by a multifocal point acoustic levitator [28]. The primary force is simulated by a numerical model combining a matrix method and the Gor'kov equation and secondary force is simulated by a numerical model based on the Finite Element Method (FEM). The forces obtained numerically are compared with those obtained by tracking the motion of the levitated droplets using a high-speed camera.

## II. EXPERIMENTAL SETUP

Water droplets are levitated and manipulated in a multifocal point acoustic levitator consisting of an array of 16 x 16 ultrasonic transducers located 110 mm above a plane reflector (Fig. 1). The transducers (Manorshi MSO-P1040H07T) have a diameter of 9.8 mm and operate at 40 kHz. The emission phase of each transducer is controlled by a Matlab script, which communicates with the driver board through serial

978-1-7281-4596-9/19/$31.00 ©2019 IEEE

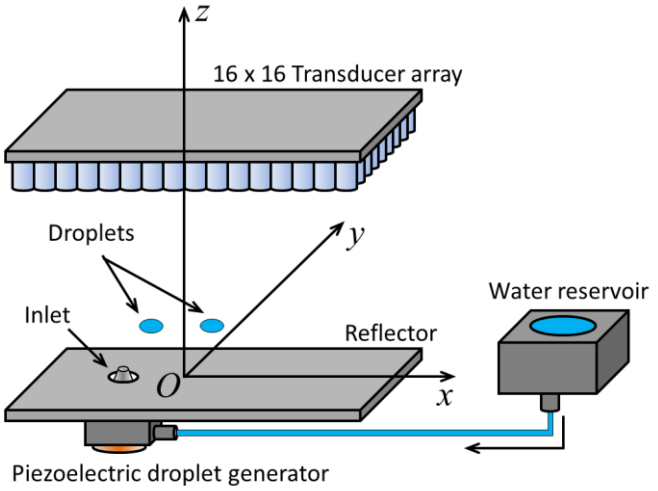


Fig. 1. Multifocal point acoustic levitator consisting of an array of 256 ultrasonic transducers and a plane reflector.

communication. The details of the multifocal point acoustic levitator can be found elsewhere [28].

In this study, two water droplets are levitated at the pressure nodes of a standing wave field established between the array and the reflector. To manipulate each droplet independently, the array of transducers is divided in two groups of transducers, forming a chess pattern, as shown in Fig. 2(a). The transducers of group 1 (red) are responsible for the levitation and the horizontal manipulation of the first droplet, whereas the manipulation of the other droplet is carried out with the other group of transducers (group 2 – blue). Each group has its own focal point, which is located over the *xy*-plane. The horizontal manipulation of each droplet is carried out by controlling the focal point of each group of transducers.

Water droplets are automatically inserted at the pressure nodes by a piezoelectric droplet generator [32]. The nozzle of the droplet generator is located on the reflector, at $(x, y, z) = (-18.5\ \text{mm}, 0, 0)$, as shown in Fig. 1.

The motion and the coalescence of the water droplets was recorded by a high-speed camera (Photron FASTCAM MINI UX50) and a tracking algorithm implemented in Matlab was used to extract the horizontal position of each droplet over time.

## III. NUMERICAL SIMULATIONS

The first step in determining the primary and secondary acoustic radiation forces acting on the levitated droplets is to simulate the acoustic pressure $p$ and particle velocity $\mathbf{u}$ distributions in the air medium. The acoustic pressure distribution generated between the array and the reflector is simulated by a modified version [28] of the matrix method [18], [33]. A typical pressure distribution simulated by the modified matrix method is shown in Fig. 2(a) (and zoomed-in Fig. 2(b)). In this example, only the transducers of the first group (red) are emitting, with its focal point located at $(x_f, y_f, z_f)$ = (7.5 mm, 0, 0). The superposition of the incident and reflected waves on the reflector generates a standing wave above the focal point, where a water droplet can be levitated at the bottom pressure node, located at a height of ≈ 2.4 mm (symbol "+" in Fig. 2(b)) above the reflector. The water droplet is then manipulated horizontally by changing the position of the focal point.

From the acoustic pressure $p$ and particle velocity $\mathbf{u}$ fields, the primary acoustic radiation force $\mathbf{F_{prim}}$ acting on the levitating droplet can be calculated by:

$$\mathbf{F_{prim}} = -\nabla U, \tag{1}$$

where

$$U = 2\pi R^3 \left[\frac{1}{3\rho_0 c_0^2}\langle p^2\rangle - \frac{\rho_0}{2}\langle \mathbf{u}\cdot\mathbf{u}\rangle\right] \tag{2}$$

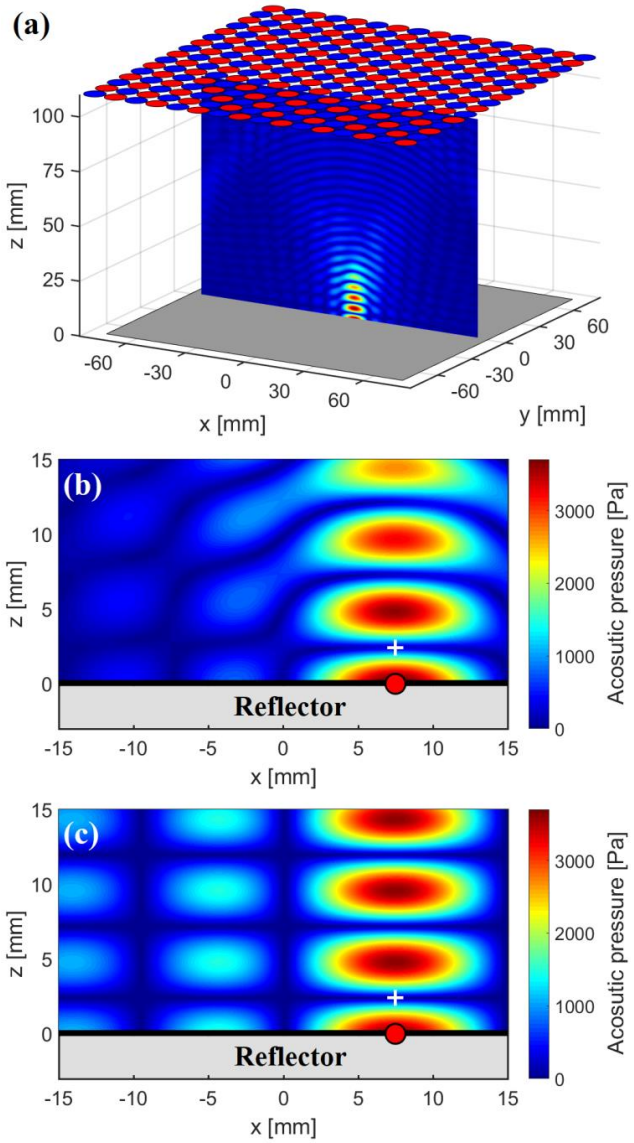


Fig. 2. Numerical simulation of the acoustic pressure distribution generated by the acoustic manipulation system. (a) Acoustic pressure distribution generated by the transducers of group 1 (red) focusing at (*x*,*y*,*z*) = (7.5 mm, 0, 0). (b) Acoustic pressure distribution determined by the modified matrix method. (c) Analytical approximation for the acoustic pressure distribution of Fig. 1(b). This distribution was calculated using (3).

is the potential of the acoustic radiation force (also called Gor'kov potential) [34]. In (2), $R$ is the droplet radius, $\rho_0$ = 1.2 kg/m$^3$ is the air density, $c_0$ = 343 m/s is the speed of sound in the air medium and the symbol $\langle \quad \rangle$ denotes time-average over one period.

To simplify the problem of determining the secondary force on the water droplets, only the $x$-component $x_f$ of the focal point coordinates is nonzero and the acoustic pressure distribution is approximated by an analytical expression representing the superposition of two counter-propagating Bessel beams, given by:

$$p = p_0 \mathrm{J}_0\left(k_r\sqrt{(x-x_f)^2+y^2}\right)cos(k_z z+\phi)cos(\omega t), \quad (3)$$

where $p_0$ is the acoustic pressure amplitude, $\omega$ is the angular frequency, $\phi$ is the spatial phase, $\mathrm{J}_0$ is the zero-order Bessel function of first kind, and $k_z$ and $k_r$ are the vertical and radial components of the wavevector, respectively. In (3), $k_z$ and $k_r$ must satisfy $k = 2\pi/\lambda = \sqrt{k_z^2 + k_r^2}$, where $\lambda$ is the acoustic wavelength. In Fig. 2(c), the acoustic pressure distribution was calculated with the analytical expression given by (3). As one can see, there is a reasonable agreement between the pressure distribution calculated by the modified matrix method (Fig. 2(b)) and that obtained by the analytical expression (Fig. 2(c)).

The primary and secondary acoustic radiation forces on water droplets are also simulated using the Finite Element Method. The simulations are carried out in the FEM software COMSOL Multiphysics and the primary and secondary forces are calculated with a procedure described by Simon et al. [35]. However, instead of considering a plane standing wave field, we assume an incident field given by (3). In COMSOL, the incident field is introduced as a background field and the water droplet is modeled as a rigid object.

Using the simulated acoustic pressure $p$ and the particle velocity $\mathbf{u}$ distributions, the acoustic radiation force on the droplet is calculated by:

$$\mathbf{F} = -\int_{S_0}\left[\frac{1}{2\rho_0 c_0^2}\langle p^2\rangle - \frac{\rho_0}{2}\langle \mathbf{u}\cdot\mathbf{u}\rangle\right]\mathbf{n}dS, \quad (4)$$

where the integral is evaluated over the droplet surface $S_0$ and $\mathbf{n}$ is the surface unit vector pointing outwards from the droplet surface.

Two finite element models were implemented in COMSOL Multiphysics. The first model, shown in Fig. 3(a), calculates the primary acoustic radiation force on a single droplet. To reduce the computation time, a symmetry condition is applied over the $xz$-plane and only half of the domain is simulated. In the model, perfectly matched layers (PML) were also employed to avoid reflections at the outer boundaries of the domain.

The second finite element model (Fig. 3(b)) calculates the secondary acoustic radiation force between two water droplets. Instead of including two spherical droplets in the model, a symmetry condition is applied over the $xz$ and $yz$ planes, which means that the model takes into account the presence of a droplet at the position $x$ and another identical droplet at the position -$x$. From the simulated fields $p$ and $\mathbf{u}$, the total acoustic radiation force $\mathbf{F_{total}}$ on the water droplet is calculated using (4). Then the secondary force $\mathbf{F_{sec}}$ is calculated using the following expression [35]:

$$\mathbf{F}_{sec} = \mathbf{F_{total}} - \mathbf{F_{prim}}. \quad (5)$$

## IV. RESULTS

In the experiments, water droplets of 1.1 mm in diameter are automatically inserted in the levitator using the piezoelectric droplet generator located at ($x$,$y$,$z$) = (-18.5 mm, 0, 0). After the insertion of the first droplet, the focal point of the first group of transducers is moved to ($x$,$y$,$z$) = (+7 mm, 0, 0) such that the droplet is transported to a trapping point located 2.4 mm above the focal point. Then the second droplet is injected and the second group of transducers manipulates the droplet to $x$ = -7 mm. A picture of the levitating droplets and the corresponding simulated Gor'kov potential after conducting this procedure is shown in Fig. 4. As shown in Fig. 4, the droplets levitate at a position of minimum Gor'kov potential, located at a height of 2.4 mm above the plane reflector.

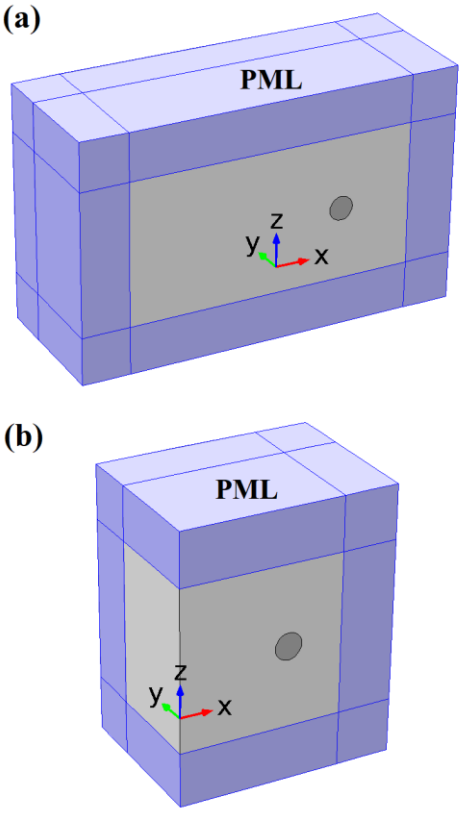


Fig. 3. Three-dimensional FEM models used to find the primary and secondary acoustic radiation forces on a water droplet. (a) Simulation of the primary acoustic radiation force on the droplet. (b) Simulation of the secondary force between two water droplets. In the model of Fig. 3(b), a symmetry boundary condition is considered over the $xz$ and $yz$ planes.

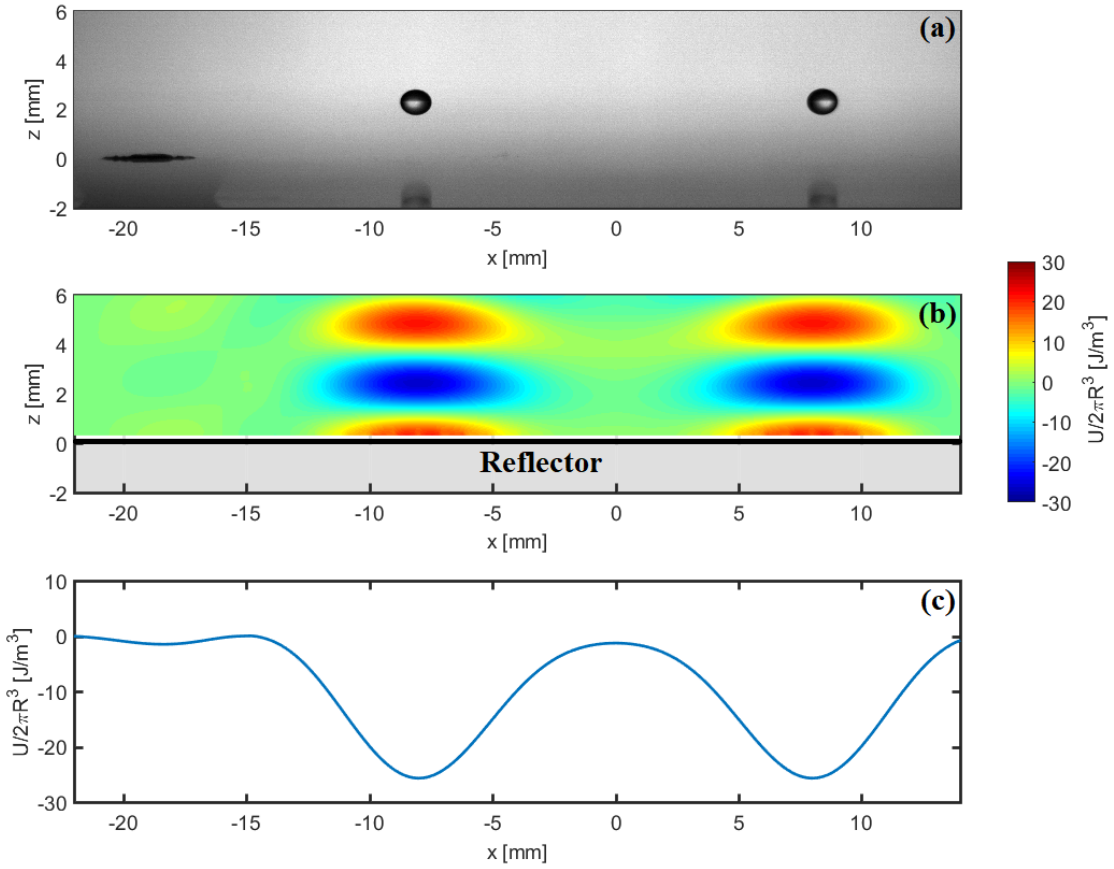


Fig. 4. Acoustic levitation of two water droplets and simulated Gor'kov potential when the transducers of group 1 (red) are focusing at $(x,y,z)$ = (+7.0 mm, 0, 0) and the transducers of group 2 (blue) focusing at $(x,y,z)$ = (-7.0 mm, 0, 0). (a) Experiment. (b) Simulated Gor'kov potential. (c) Simulated Gor'kov potential along the $x$ direction for $z$ = 2.4 mm.

After the stabilization of the water droplets at $x$ = +7 mm and $x$ = -7 mm, the first and second focal points are slowly moved to $x$ = +5.08 mm and $x$ = -5.08 mm, respectively, causing the droplets to merge. Although the focal points are separated by a distance of 10.16 mm, the experiments were repeated multiple times and in all the cases the droplets merged when the focal points reached $x$ = +5.08 mm and $x$ = -5.08 mm. The simulated Gor'kov potential for this condition is shown in Fig. 5. According to this simulation, there is a minimum of Gor'kov potential at $x$ = +2.7 mm and another at $x$ = -2.7 mm, as indicated by the symbol "+" in Fig. 5(a). In principle, one would expect a stable levitation of the droplets at these two positions, but the presence of the secondary acoustic radiation force causes an attractive force between the droplets, making them to coalesce.

A typical coalescence process between two water droplets is shown in Fig. 6. The experimental results of Fig. 6 were obtained by recording the merging of the water droplets with a high-speed camera. The horizontal position of each droplet before and after the coalescence process is shown in Fig. 6(a) and the sequence of frames of this process is presented in Fig. 6(b). As shown in Fig. 6(a), there is an increasing acceleration between the droplets before they coalesce at $t$ = 0.33 s. After merging the water droplets the resulting droplet presents a complex horizontal motion, which is governed by the shape of the Gor'kov potential.

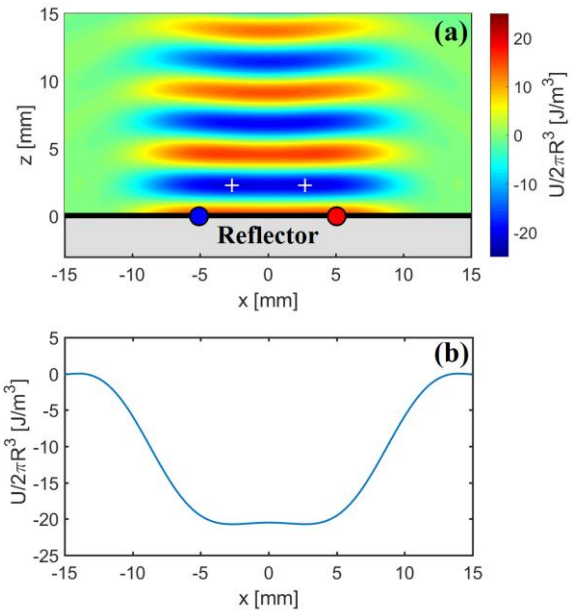


Fig. 5. Simulated Gor'kov potential when the transducers of group 1 (red) are focusing at $(x,y,z)$ = (+5.08 mm, 0, 0) and the transducers of group 2 (blue) focusing at $(x,y,z)$ = (-5.08 mm, 0, 0). (a) Gor'kov potential over the $xz$-plane. (b) Potential along the $x$-axis for z = 2.4 mm.

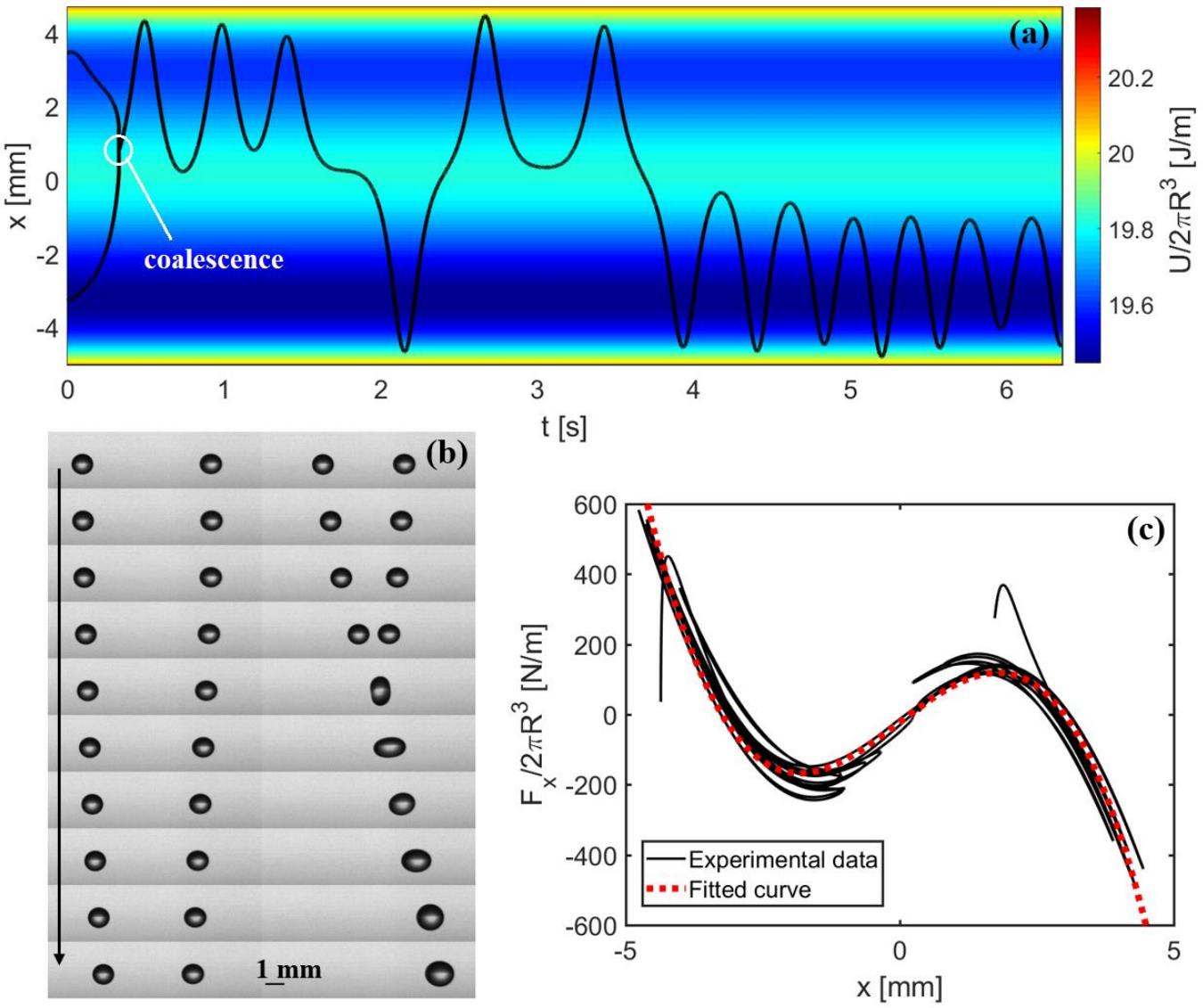


Fig. 6. Reconstruction of the primary acoustic radiation force using the experimental droplet position over time. (a) Horizontal position of the water droplets over time and the reconstructed potential of the acoustic radiation force. (b) Sequence of frames of the coalescence process. The time between frames is 25 ms. (c) Horizontal component of the acoustic radiation force as a function of $x$.

Neglecting drag forces and assuming that only the primary acoustic radiation force is acting on the resulting droplet, we can say that the droplet horizontal acceleration is given by $a_x = F_x/m$, where $F_x$ is the horizontal component of the primary acoustic radiation force and $m$ is the droplet mass. From the experimental horizontal position of the droplet after the coalescence, we can plot the horizontal force on the droplet as a function of its horizontal position (Fig. 6(c)). Then, by fitting a polynomial curve of degree 3, we obtain the red dashed line of Fig. 6(c), which represents the horizontal component of the primary acoustic radiation force on the droplet as a function of $x$. A polynomial of degree 3 was chosen because it is the lowest-order polynomial that accurately fits the experimental data. The comparison between the horizontal primary acoustic radiation force determined experimentally with the numerical force obtained by the FEM and by the matrix method is shown in Fig. 7.

The FEM models of Figs. 3(a) and 3(b) were also used for calculating the primary, secondary and total force on a spherical water droplet located at a horizontal position $+x$. The secondary force acting on the sphere is caused by the wave scattered by another sphere located at a position $-x$. According to the simulated result of Fig. 8, the secondary force is very small when the separation distance between the water droplets is greater than 4 mm ($x$ = 2 mm). For smaller distances, the secondary force rapidly increases when spheres approach each other. When the droplets become sufficiently close, the secondary force causes a strong attractive acceleration between the droplets, which contributes with the coalescence process. The simulated results of Fig. 8 are in agreement with our experimental observations.

## V. CONCLUSIONS

The manipulation capability of the levitation system was demonstrated by transporting and merging water droplets in

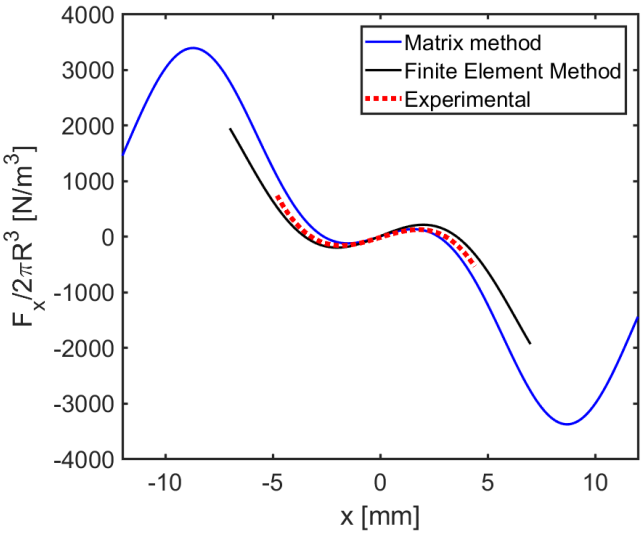


Fig. 7. Horizontal primary acoustic radiation force on a water droplet when the transducers of group 1 (red) are focusing at $(x,y,z)$ = (+5.08 mm, 0, 0) and the transducers of group 2 (blue) focusing at $(x,y,z)$ = (-5.08 mm, 0, 0).

mid-ar. The primary and secondary acoustic radiation forces acting on the levitated droplets were also investigated numerically and experimentally. The experimental and numerical results show that the secondary force is small for large distances between the droplets. However, when the droplets are sufficiently close to each other, the secondary force dominates over the primary force, causing a strong attractive acceleration between the droplets. A good understanding of the radiation forces involved in the contactless manipulation of droplets will be of vital importance for designing reliable acoustic levitation systems for liquid processing in the areas of biology, pharmacy and chemistry.

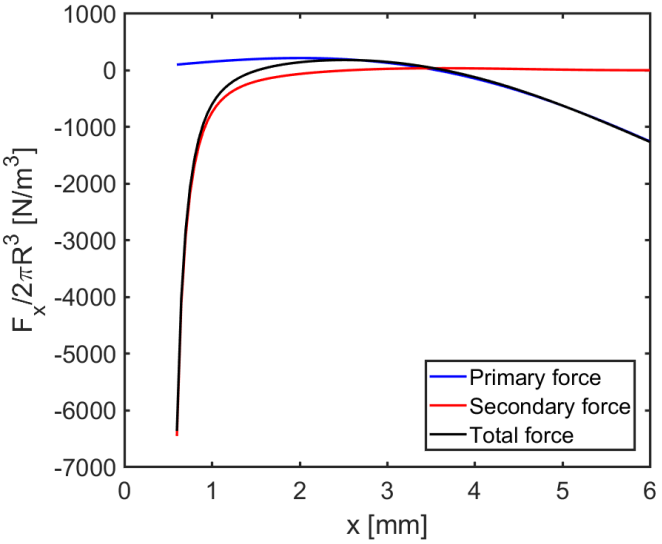


Fig. 8. Simulated primary, secondary and total force on a levitating water sphere located at a horizontal position $x$. The secondary force is caused by the wave scattering of an identical water droplet located at a position $-x$. The forces were calculated by FEM simulations and considering spherical water droplets of radius $R$ = 0.55 mm.

## REFERENCES

[1] E. H. Brandt, "Acoustic physics. Suspended by sound.," *Nature*, vol. 413, no. 6855, pp. 474–475, 2001.

[2] M. A. B. Andrade, N. Pérez, and J. C. Adamowski, "Review of Progress in Acoustic Levitation," *Brazilian J. Phys.*, vol. 48, no. 2, pp. 190–213, 2018.

[3] R. T. Beyer, "Radiation pressure - The history of a mislabled tensor," *J. Acoust. Soc. Am.*, vol. 63, no. 4, pp. 1025–1030, 1978.

[4] H. Bruus, "Acoustofluidics 7: The acoustic radiation force on small particles," *Lab Chip*, vol. 12, no. 6, pp. 1014–1021, 2012.

[5] V. Vandaele, A. Delchambre, and P. Lambert, "Acoustic wave levitation: Handling of components," *J. Appl. Phys.*, vol. 109, no. 12, p. 124, 2011.

[6] M. A. B. Andrade, A. L. Bernassau, and J. C. Adamowski, "Acoustic levitation of a large solid sphere," *Appl. Phys. Lett.*, vol. 109, no. 4, art. no. 044101, 2016.

[7] D. Zang, Y. Yu, Z. Chen, X. Li, H. Wu, and X. Geng, "Acoustic levitation of liquid drops: Dynamics, manipulation and phase transitions," *Adv. Colloid Interface Sci.*, vol. 243, pp. 77–85, 2017.

[8] D. Zang, K. Lin, L. Li, Z. Chen, X. Li, and X. Geng, "Acoustic levitation of soap bubbles in air: Beyond the half-wavelength limit of sound," *Appl. Phys. Lett.*, vol. 110, no. 12, art. no. 121602, 2017.

[9] W. J. Xie, C. D. Cao, Y. J. Lü, Z. Y. Hong, and B. Wei, "Acoustic method for levitation of small living animals," *Appl. Phys. Lett.*, vol. 89, no. 21, art. no. 214102, 2006.

[10] E. H. Trinh, "Compact acoustic levitation device for studies in fluid dynamics and material science in the laboratory and microgravity," *Rev. Sci. Instrum.*, vol. 56, no. 11, pp. 2059–2065, 1985.

[11] W. J. Xie and B. Wei, "Parametric study of single-axis acoustic levitation," *Appl. Phys. Lett.*, vol. 79, no. 6, pp. 881–883, 2001.

[12] M. A. B. Andrade, F. C. Buiochi, and J. Adamowski, "Finite element analysis and optimization of a single-axis acoustic levitator," *IEEE Trans. Ultrason. Ferroelectr. Freq. Control*, vol. 57, no. 2, pp. 469–479, 2010.

[13] J. K. R. Weber, C. A. Rey, J. Neuefeind, and C. J. Benmore, "Acoustic levitator for structure measurements on low temperature liquid droplets," *Rev. Sci. Instrum.*, vol. 80, no. 8, art. no. 083904, 2009.

[14] Y. Ochiai, T. Hoshi, and J. Rekimoto, "Three-dimensional mid-air acoustic manipulation by ultrasonic phased arrays," *PLoS One*, vol. 9, no. 5, p. e97590, 2014.

[15] A. Marzo, A. Barnes, and B. W. Drinkwater, "TinyLev: A multi-emitter single-axis acoustic levitator," *Rev. Sci. Instrum.*, vol. 88, no. 8, art. no. 085105, 2017.

[16] A. Marzo, T. Corkett, and B. W. Drinkwater, "Ultraino: an Open Phased-Array System for Narrowband Airborne Ultrasound Transmission," *IEEE Trans. Ultrason. Ferroelectr. Freq. Control*, vol. 65, no. 1, pp. 102–111, 2018.

[17] A. Marzo and B. W. Drinkwater, "Holographic acoustic tweezers," *Proc. Natl. Acad. Sci.*, vol. 116, no. 1, pp. 84–89, 2019.

[18] M. A. B. Andrade, N. Perez, F. Buiochi, and J. C. Adamowski, "Matrix method for acoustic levitation simulation," *IEEE Trans. Ultrason. Ferroelectr. Freq. Control*, vol. 58, no. 8, pp. 1674–1683, 2011.

[19] D. Foresti, M. Nabavi, M. Klingauf, A. Ferrari, and D. Poulikakos, "Acoustophoretic contactless transport and handling of matter in air," *Proc. Natl. Acad. Sci.*, vol. 110, no. 31, pp. 12549–12554, 2013.

[20] R. Kashima, D. Koyama, and M. Matsukawa, "Two-dimensional noncontact transportation of small objects in air using flexural vibration of a plate," *IEEE Trans. Ultrason. Ferroelectr. Freq. Control*, vol. 62, no. 12, pp. 2161–2168, 2015.

[21] S. Santesson and S. Nilsson, "Airborne chemistry: Acoustic levitation in chemical analysis," *Anal. Bioanal. Chem.*, vol. 378, no. 7, pp. 1704–1709, 2004.

[22] C. J. Benmore and J. K. R. Weber, "Amorphization of Molecular Liquids of Pharmaceutical Drugs by Acoustic Levitation," *Phys. Rev. X*, vol. 1, no. 1, art. no. 011004, 2011.

[23] T. Vasileiou, D. Foresti, A. Bayram, D. Poulikakos, and A. Ferrari, "Toward Contactless Biology: Acoustophoretic DNA Transfection.,"

*Sci. Rep.*, vol. 6, no. December 2015, art. no. 20023, 2016.

[24] S. Tsujino and T. Tomizaki, "Ultrasonic acoustic levitation for fast frame rate X-ray protein crystallography at room temperature," *Sci. Rep.*, vol. 6, no. 1, art. no. 25558, 2016.

[25] R. H. Morris, E. R. Dye, D. Axford, M. I. Newton, J. H. Beale, and P. T. Docker, "Non-Contact Universal Sample Presentation for Room Temperature Macromolecular Crystallography Using Acoustic Levitation," *Sci. Rep.*, vol. 9, art. no. 12431, 2019.

[26] S. Santesson *et al.*, "Airborne chemistry coupled to Raman spectroscopy," *Anal. Chem.*, vol. 75, no. 9, pp. 2177–2180, 2003.

[27] A. Watanabe, K. Hasegawa, and Y. Abe, "Contactless fluid manipulation in air: Droplet coalescence and active mixing by acoustic levitation," *Sci. Rep.*, vol. 8, art. no. 10221, 2018.

[28] M. A. B. Andrade, T. S. A. Camargo, and A. Marzo, "Automatic contactless injection, transportation, merging, and ejection of droplets with a multifocal point acoustic levitator," *Rev. Sci. Instrum.*, vol. 89, no. 12, art. no. 125105, 2018.

[29] V. F. K. Bjerknes, *Fields of Force*. New York: Columbia University, 1906.

[30] L. A. Crum, "Bjerknes forces on bubbles in a stationary sound field," *J. Acoust. Soc. Am.*, vol. 57, no. 6, pp. 1363–1370, 1975.

[31] G. T. Silva and H. Bruus, "Acoustic interaction forces between small particles in an ideal fluid," *Phys. Rev. E - Stat. Nonlinear, Soft Matter Phys.*, vol. 90, no. 6, art. no. 063007, 2014.

[32] D. M. Harris, T. Liu, and J. W. M. Bush, "A low-cost, precise piezoelectric droplet-on-demand generator," *Exp. Fluids*, vol. 56, no. 4, p. 83, 2015.

[33] A. Stindt, M. A. B. Andrade, M. Albrecht, J. C. Adamowski, U. Panne, and J. Riedel, "Experimental and numerical characterization of the sound pressure in standing wave acoustic levitators," *Rev. Sci. Instrum.*, vol. 85, no. 1, art. no. 015110, 2014.

[34] L. P. Gor'kov, "On the Forces Acting on a Small Particle in an Acoustical Field in an Ideal Fluid," *Solviet Physics Doklady*, vol. 6. pp. 773–775, 1962.

[35] G. Simon, M. A. B. Andrade, M. P. Y. Desmulliez, M. O. Riehle, and A. L. Bernassau, "Numerical Determination of the Secondary Acoustic Radiation Force on a Small Sphere in a Plane Standing Wave Field," *Micromachines*, vol. 10, p. 431, 2019.